

FEDSM-ICNMM2010-' \$&+,

PIV MEASUREMENTS OF THE TURBULENT SECONDARY FLOW IN A THREE-DIMENSIONAL WALL JET

Lhendup Namgyal

Department of Mechanical Engineering
 University of New Brunswick
 Fredericton, New Brunswick
 Canada
 Email: q8196@unb.ca

Joseph W. Hall*

Department of Mechanical Engineering
 University of New Brunswick
 Fredericton, New Brunswick
 Canada
 Email: jwhall@unb.ca

ABSTRACT

The lateral half width of the turbulent three-dimensional wall jet is typically five to eight times larger than the vertical half width normal to the wall. Although, the reason for this behavior is not fully understood, it is known to be caused by strong secondary flows that develop in the jet due to presence of the wall. The source of the secondary flow in the jet has been attributed previously with both mean vorticity reorientation and to anisotropy in the Reynolds normal stresses, but until now there have been no measurements of these quantities in this flow. Particle Image Velocimetry (PIV) measurements are used herein to measure the Reynolds stresses that contribute to the secondary flow in a turbulent three-dimensional wall jet formed using a circular contoured nozzle with exit Reynolds number of 250,000. In particular, the Reynolds shear stress, \overline{vw} was found to be significantly smaller throughout the jet than the differences in the Reynolds normal stresses ($\overline{v^2} - \overline{w^2}$).

u	Streamwise fluctuating velocity, m/s
v	Normal fluctuating velocity, m/s
w	Lateral fluctuating velocity, m/s
\overline{uv}	Reynolds shear stress, m^2/s^2
\overline{vw}	Reynolds shear stress, m^2/s^2
$\overline{u^2}$	Streamwise normal stress, m^2/s^2
$\overline{v^2}$	Vertical normal stress, m^2/s^2
$\overline{w^2}$	Lateral normal stress, m^2/s^2
x	Streamwise coordinate, m
y	Vertical coordinate, m
z	Lateral coordinate, m
y_{max}	Height of U_{max} , m
$y_{1/2}$	Vertical jet half-width, m
$z_{1/2}$	Lateral jet half-width, m
Ω_x	Mean streamwise vorticity, $1/s$
Ω_y	Mean normal vorticity, $1/s$
Ω_z	Mean lateral vorticity, $1/s$

NOMENCLATURE

D	Exit diameter, m
U	Mean streamwise velocity, m/s
U_{max}	Maximum streamwise velocity, m/s
V	Mean normal velocity, m/s
W	Mean Lateral velocity, m/s

INTRODUCTION

Three-dimensional wall jets are formed when a fluid flows from a finite width opening tangentially along a wall, as shown in Fig. 1. Wall jets have a diverse range of engineering applications, such as cooling of gas turbine combustor walls and in ventilation systems. The most common application of wall jets from daily life is likely the automobile windshield defroster.

*Address all correspondence to this author.

One of the most noteworthy features of three-dimensional wall jets is that the lateral spread rate is five to eight times greater than the vertical spread rate normal to the wall in the far-field [1, 2, 3, 4, 5, 6, 7, 8], however, the cause of the large lateral spread rate in three-dimensional wall jets is not fully understood.

Launder and Rodi [3], noted that the large lateral growth had to be due to mean secondary flows in the jet and examined the governing equations for the transport of mean streamwise vorticity for steady, incompressible flow:

$$\underbrace{\frac{D\Omega_x}{Dt}}_A = \underbrace{\Omega_x \frac{\partial U}{\partial x}}_B + \underbrace{\Omega_y \frac{\partial U}{\partial y} + \Omega_z \frac{\partial U}{\partial z}}_C + \underbrace{\frac{\partial^2}{\partial y \partial z} (\overline{v^2} - \overline{w^2})}_D + \underbrace{\left(\frac{\partial^2}{\partial z^2} - \frac{\partial^2}{\partial y^2} \right) \overline{vw}}_E + \underbrace{v \left(\frac{\partial^2 \Omega_x}{\partial x^2} + \frac{\partial^2 \Omega_x}{\partial y^2} + \frac{\partial^2 \Omega_x}{\partial z^2} \right)}_F \quad (1)$$

Where

- A – Transport of streamwise vorticity
- B – Amplification of vorticity by vortex-stretching
- C – Vorticity production by vortex-line bending
- D – Vorticity production by gradient in Reynolds stresses
- E – Vorticity production by gradient in Reynolds shear stresses
- F – Viscous diffusion of vorticity

Launder and Rodi [3] stated that one possible source of streamwise vorticity in the three-dimensional wall jet was due to the vortex reorientation (Term C). They suggested that this caused the formation of the two counter-rotating regions of mean streamwise vorticity positioned one on top of another on both side of the jet centerline; these regions were thought to drive the mean flow down into the wall and eject it laterally outward thereby causing the large lateral growth. Several later experiments confirmed the presence of these regions [9, 10, 11, 12, 13, 14], however they consisted of a larger diffuse region above a smaller, stronger near wall region on either side of the jet centerline. The regions were oriented appropriately to drive the flow down and laterally outward.

Launder and Rodi [3] also suggested that streamwise vorticity could be generated because of gradients in the Reynolds stresses (Term D and E), so-called turbulence generated secondary flow. They argued that the production of streamwise vorticity due to gradients in the normal stresses (Term D) should be on the same order as the vortex-tilting terms and should act to reinforce the secondary flow due to vortex tilting in the far-field. This was later examined by Craft and Launder [5] who numerically examined the three-dimensional wall jet and noted that a

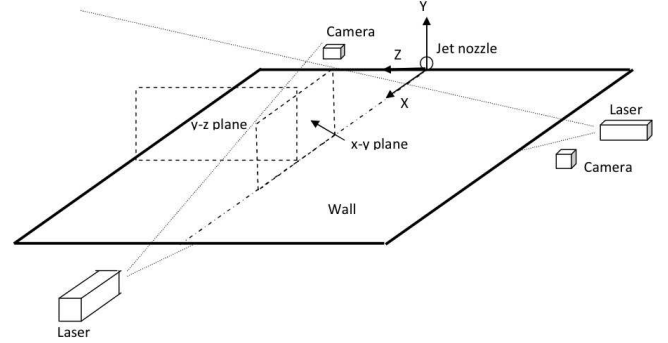


FIGURE 1. Schematic of experimental apparatus showing the two PIV configurations.

similar vortex-tilting process should occur in the laminar jet as in the turbulent case. They simulated a laminar three-dimensional wall jet and found that the lateral growth was significantly less than the turbulent case; from this they argued that the vortex-tilting process alone was not sufficient to cause the large lateral spreading that occurs in the turbulent wall jet, and thus it must be due to gradients in the Reynolds stresses.

Unfortunately we have little information about the relative proportions of the Reynolds stresses that contribute to the secondary flow in the three-dimensional wall jet (\overline{vw} , $\overline{v^2}$ and $\overline{w^2}$), let alone the size of terms D and E in (1). Thus, the goal of the present paper is to use PIV measurements to measure the aforementioned Reynolds stresses in the hopes of better understanding the source of turbulent generated secondary flow in the three-dimensional wall jet. Owing to the complex nature of turbulence in the jet, the present paper will focus only on profiles of the turbulent velocities rather than the full flow-field. These measurements will be performed in the far-field ($x/D = 50$) of a turbulent three-dimensional wall jet formed using a circular contoured nozzle with an exit Reynolds number of 250,000.

EXPERIMENTAL SETUP

The air flow to the jet was supplied by a 6.5HP, single stage centrifugal blower. The flow is conditioned in a 0.9m x 0.9m x 0.9m settling chamber with three 10mm mesh screens. The flow from the settling chamber is then passed through a flow straightener placed inside a 0.20m diameter pipe. Finally, the air flows through a contoured nozzle with an area contraction ratio of 28:1. The nozzle has a fifth order polynomial profile so as to produce a top hat exit velocity profile within 0.25% turbulence intensity. The jet Reynolds number at the exit was set to 2.5×10^5 . Upon exiting the nozzle, the air flows tangentially along a 2.29 m x 2.08 m horizontal wall forming the three-dimensional wall jet.

The velocity field was acquired using a *LaVision* PIV sys-

tem. The flow was seeded using olive oil droplets, generated from a Laskin type atomizer. This produced a mean particle diameter of $3\mu\text{m}$. A Solo 120XT Nd-Yag laser having a pulse energy of 120mJ was used to illuminate the flow. The images were acquired by a 12 bit resolution CCD camera (*LaVision Image intense*) with a resolution of 1376×1040 pixels. The double frame instantaneous images were processed using *LaVision Flow Manager (DaVis 7.2 version)*. In the data processing, multipass decreasing interrogation window sizes of 32×32 with 75% overlap is adopted and to avoid the peak locking effect [15] and a normalized correlation function was used and then the processed data is reconstructed using the Whittaker algorithm.

Both the laser and the camera were arranged to facilitate measurement in both the transverse ($y-z$ plane) and streamwise ($x-y$ plane) plane, shown in Fig. 1. Ten sets of measurement positions were employed in the streamwise ($x-y$) plane, starting from the centerline of the jet with an interval of $2D$ up to $z_{1/2}$ and $3D$ beyond it. Sample instantaneous vector fields for each configuration are shown in Fig. 2 and 3. These sets of measurements were then aligned to generate three profiles of the streamwise component in the lateral direction. In order to reduce the measurement uncertainty, 6000 independent pairs of images were taken. Since every vector field can be considered to be an independent event [16], the uncertainties at the 95% confidence level associated with mean streamwise velocity at the center of the jet at y_{max} , and $y_{1/2}$ were determined to be 0.7% and 1.36% respectively.

EXPERIMENTAL RESULTS

The profiles of the mean and turbulent velocities measured normal to the wall at the jet centerline are shown in Figs. 4 and 5, respectively. Similar profiles measured across the jet and parallel to the wall are shown in Figs. 6 and 7, respectively. In all cases, the results have been normalized by the local maximum streamwise velocity, U_{max} and respective jet half-width. In both cases, the mean streamwise velocity profiles exhibit classical wall jet behavior and are in quite good agreement with the values measured by Sun [6]. Sun used single and cross-wire anemometry to determine the mean and turbulent profiles in a three-dimensional wall jet formed using a contoured nozzle at $x/D = 40$ for a Reynolds number of 108,000. At the jet centerline, the present measurements indicated that mean component of velocity normal to the wall, V , is approximately 5% of U_{max} and negative. This suggests that the wall jet is entraining ambient mass and directing it downward. When one examines the mean profiles measured across the jet, it can be observed that this mass is moved laterally away from the jet centerline, as indicated by the large values of W (as high as 20% of U_{max}). At this location V is approximately zero suggesting that the principal source of entrained mass occurs at the center of the jet. This process is consistent with the model for the three-dimensional wall-jet de-

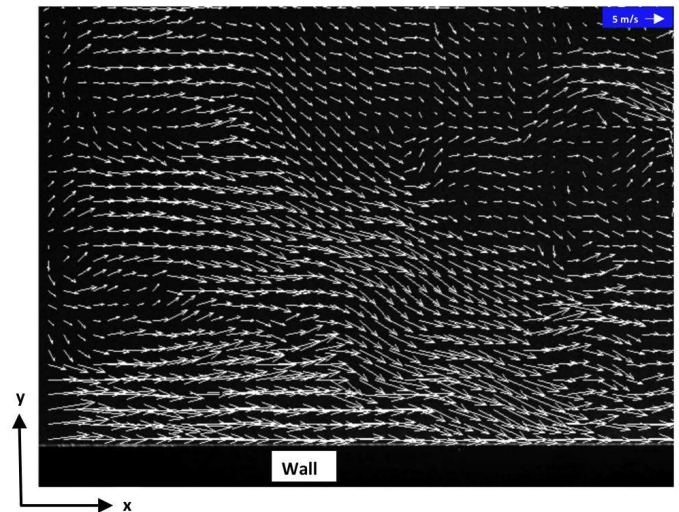


FIGURE 2. Vector field showing instantaneous streamwise velocity in $x-y$ plane. Only 1 in 4 vectors are shown for clarity.

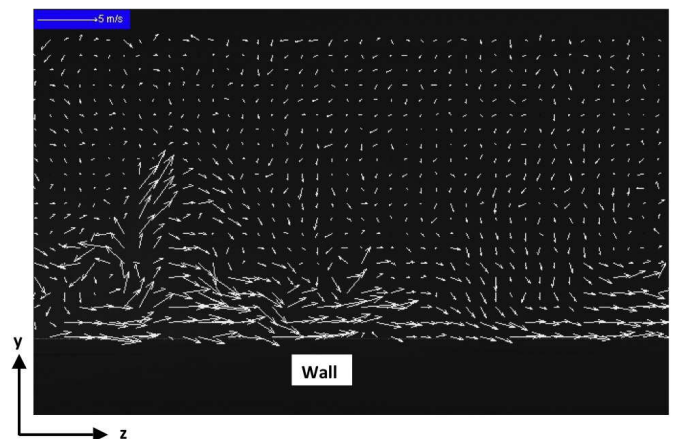


FIGURE 3. Vector field showing instantaneous lateral velocity in $y-z$ plane. Only 1 in 4 vectors are shown for clarity.

velopment put forth by Launder and Rodi [3]. The large value of the lateral velocity away from the centerline demonstrates that measurements at the jet centerline are not fully indicative of the dominant turbulent processes in this flow.

Although the mean flow profiles are in good agreement with Sun [6], there are some differences in the turbulent profiles measured at the jet centerline, as shown in Fig. 5. In particular, the measurements of all three turbulence components measured here are in good agreement near the wall, but are somewhat higher than observed by Sun away from the wall. This is most likely due to Sun's turbulent profile having not fully reached the self-

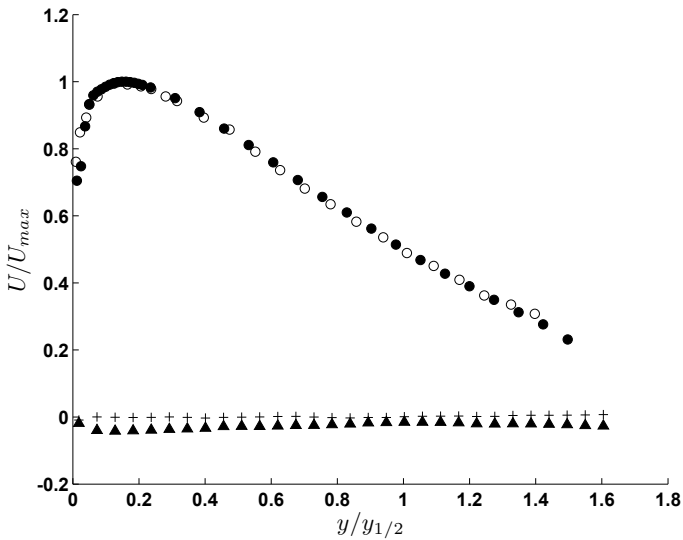


FIGURE 4. Profiles of normalized mean velocity measured at the jet centerline: (●) U , (○) U [6], (▲) V , and (+) W .

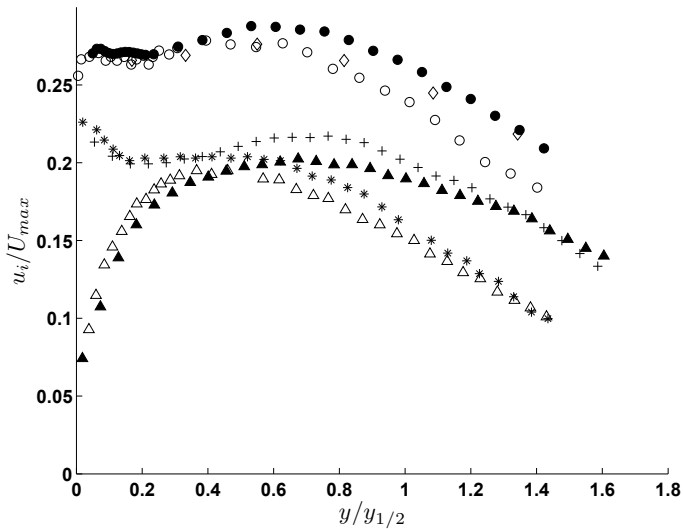


FIGURE 5. Profiles of normalized turbulent velocity measured at the jet centerline: (●) u , (◇) u PHWA [7], (○) u [6], (▲) v , (△) v [6], (+) w , and (*) w [6].

preserving state by $x/D = 40$, as it is known that the turbulence profiles take longer to develop into an equilibrium state than the mean velocity profiles. This behavior could also be somewhat attributed to the Reynolds number differences between the two jets or to the known under prediction of conventional hot-wire measurements when the local turbulence intensity is high. The under prediction of conventional HWA in the outer region of the three-

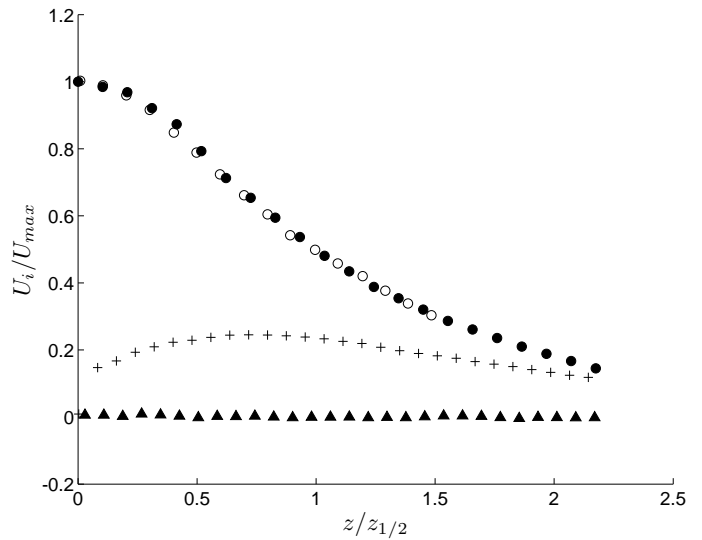


FIGURE 6. Profiles of normalized mean velocity measured at y_{max} : (●) U , (○) U [6], (▲) V , and (+) W .

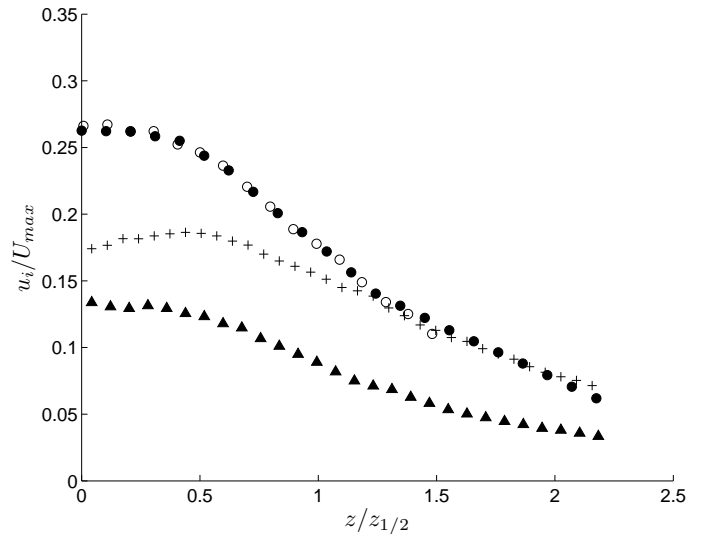


FIGURE 7. Profiles of normalized turbulent velocity measured at y_{max} : (●) u , (○) u [6], (▲) v , and (+) w .

dimensional turbulent wall jet has been investigated by Venas *et al.* [7]. They compared the results of two and three-dimensional wall jet measured using Pulsed Hot-Wire Anemometry (PHWA) with conventional Hot-Wire Anemometry (HWA) and with Laser Doppler Anemometry (LDA) for a two-dimensional wall jet. The PHWA turbulent profiles from Venas *et al.* at the centerline are compared to the present data in Fig. 5, and they are closer to the turbulent profiles obtained here than those obtained via conven-

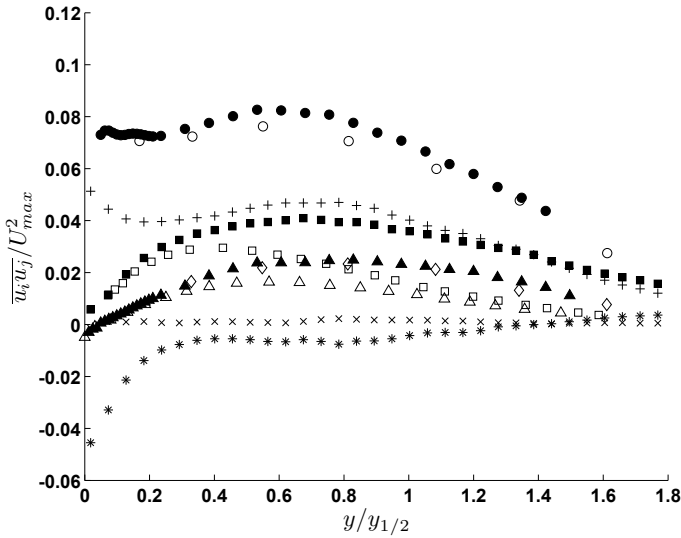


FIGURE 8. Profiles of normalized Reynolds Stresses on the jet centerline: (●) $\overline{u'u'}$, (○) $\overline{u'u'}$ PHWA [7], (▲) $\overline{v'v'}$, (△) $\overline{v'v'}$ [17], (◇) $\overline{v'v'}$ PHWA [7], (+) $\overline{w'w'}$, (x) $\overline{v'w'}$, (■) $\overline{v'v'}$, (□) $\overline{v'v'}$ [17], and (*) $\overline{v^2 - w^2}$.

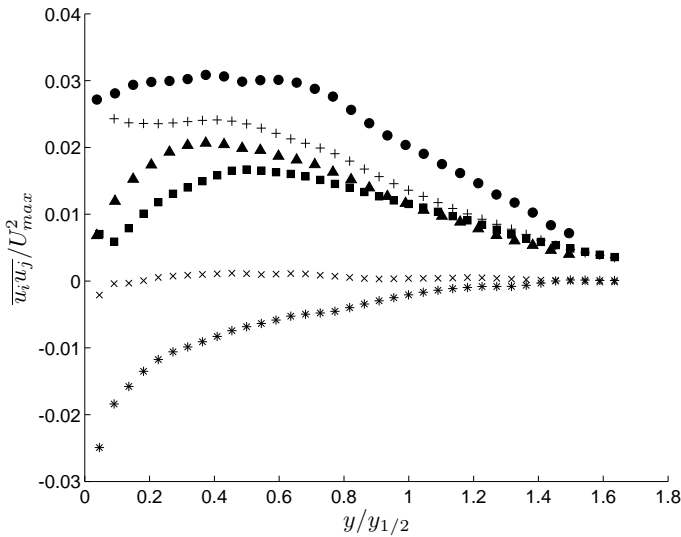


FIGURE 9. Profiles of normalized Reynolds stresses at $z_{1/2}$: (●) $\overline{u'u'}$, (▲) $\overline{v'v'}$, (+) $\overline{w'w'}$, (x) $\overline{v'w'}$, (■) $\overline{v'v'}$, and (*) $\overline{v^2 - w^2}$.

tional HWA. The streamwise fluctuations measured across the jet at y_{max} , though, are in good agreement with Sun.

The profiles of the normalized turbulent velocities measured at jet centerline and y_{max} indicates that the streamwise turbulent velocity component is dominant. At the jet centerline, the lateral turbulent velocity component is much higher near the wall than the normal turbulent velocity, likely due to the damping effect of

the wall. However, away from the wall, v is higher value than w ; this is likely associated with the downward mean entrainment of ambient fluid that occurs at the jet centerline. In the measurement across the jet at y_{max} , the lateral turbulent velocity, w , is dominant over the normal turbulent velocity, v , over the entire profile. The disparity in u and w shows the anisotropic behavior of the turbulence in the jet, particularly near the wall. This will be further examined by computing the Reynolds normal and shear stresses in the jet.

Profiles of the Reynolds stresses measured at the jet centerline are shown in Fig. 8. Of the six Reynolds stresses, only $\overline{u'w'}$ was not measured here, although it has been quantified and discussed previously by Hall and Ewing [8]. The Reynolds stress measurements of $\overline{u'v'}$ and $\overline{v^2}$ are compared to previous HWA [17] and PHWA [7] data and found to be in good agreement. Again, the current data is slightly higher than the HWA data, likely for the same reasons discussed earlier. It is clear that at the jet centerline, $\overline{u^2}$ makes the largest contribution to the Reynolds stress field. This is not surprising as the mean streamwise velocities at the centerline are much larger than V or W . The $\overline{w^2}$ values are higher than $\overline{v^2}$ at the jet centerline illustrating the high level of turbulent anisotropy at this location. The magnitude of the shear-stress term, $\overline{v'w'}$, is quite small compared to the other Reynolds stresses in the jet.

In order to improve our understanding of the source of the turbulence generated secondary flow in the jet and the relative size of the contributions in (1), the difference in the normal stresses ($\overline{v^2 - w^2}$) are compared to the $\overline{v'w'}$ shear stress term in Fig. 8. It is clear that ($\overline{v^2 - w^2}$) is significantly larger than $\overline{v'w'}$ at the jet centerline, particularly near the wall. Although we have no information about the spatial gradients, this suggests that Term D is the dominant source in (1).

As the mean velocity profiles indicated that the physics are not fully captured at the jet centerline, profiles of the Reynolds stresses obtained at $z_{1/2}$ and measured normal to the wall are shown in Fig. 9. At this location, the normal stresses $\overline{u^2}$ are still dominant but are now closer in magnitude to $\overline{w^2}$, again likely due to the lateral transport of flow away from the jet centerline. The $\overline{v^2}$ term is significantly smaller than $\overline{w^2}$ near the wall and this causes the difference between the two to remain large, in particular, much larger than $\overline{v'w'}$. Again, although we have no information as of yet about the gradients, it is quite likely that it is anisotropy in the normal stresses (Term D) that makes the largest contribution to the turbulence generated secondary flow at this location.

A similar comparison is made for the Reynolds stresses profiles measured parallel to the wall at y_{max} and $y_{1/2}$, shown in Figs. 10 and 11. Again the agreement in the profiles of $\overline{u^2}$ with the PHWA data is quite good. At both locations, $\overline{u^2}$ makes the largest contribution to the Reynolds stresses. The maximum

occurs on the jet centerline and decays with increasing distance from the centerline. Across the jet, the $\overline{w^2}$ term is dominant over the $\overline{v^2}$, and overtakes \overline{uv} in both cases at around $z/z_{1/2} = 0.5$. The shear stress term \overline{vw} is in all cases quite weak with respect to the contributions from the other Reynolds stresses. The differences in the normal stresses, $(\overline{v^2} - \overline{w^2})$, are also compared at both locations. At both locations, this term is significantly larger than \overline{vw} . Taken together, these results indicate that the differences in the normal stresses $(\overline{v^2} - \overline{w^2})$ are larger in magnitude than \overline{vw} throughout the jet. This suggests that D is the dominant source term in (1) throughout the jet.

CONCLUDING REMARKS

The development of the three-dimensional wall jet exiting from a contoured nozzle was investigated using PIV in the far field region. Measurements of all three-components of the mean flow velocity and 5 of this 6 Reynolds stress components were performed here. At all positions, the contribution from \overline{vw} was weak compared to the other Reynolds stresses. The differences in the Reynolds normal stresses, $(\overline{v^2} - \overline{w^2})$, was largest near the wall indicating that the wall is the cause of the anisotropy in the turbulence. Moreover, the magnitude of $\overline{v^2} - \overline{w^2}$ was significantly greater than \overline{vw} at all positions; this suggests that Term D in (1) is the cause of the larger lateral growth in the three-dimensional wall jet. However, this cannot be said with certainty as the determination of the source requires calculation of double spatial gradients associated with these terms. Examination of the contours of the full flow field and calculation of these double spatial gradients is underway.

REFERENCES

- [1] Sforza, P. M., and Herbst, G., 1970. "A study of three-dimensional, incompressible, turbulent wall jets". *AIAA Journal*, **8**, pp. 276–283.
- [2] Davis, M. R., and Winarto, H., 1980. "Jet diffusion from a circular nozzle above a solid plane". *Journal of Fluid Mechanics*, **101**, pp. 193–218.
- [3] Launder, B. E., and Rodi, W., 1983. "The turbulent wall jet-measurements and modelling". *Annual Review of Fluid Mechanics*, **15**, pp. 429–459.
- [4] Sullivan, P., and Pollard, A., 1996. "Coherent structure identification from the analysis of hot-wire data". *Measurement Science and Technology*, **7**, pp. 1498–1516.
- [5] Craft, T. J., and Launder, B. E., 2001. "On the spreading mechanism of the three-dimensional turbulent wall jet". *Journal of Fluid Mechanics*, **435**, pp. 305–326.
- [6] Sun, H., 2002. "The effect of initial conditions on the development of the three-dimensional wall jet". PhD thesis, McMaster University, Hamilton, Ontario, Canada.

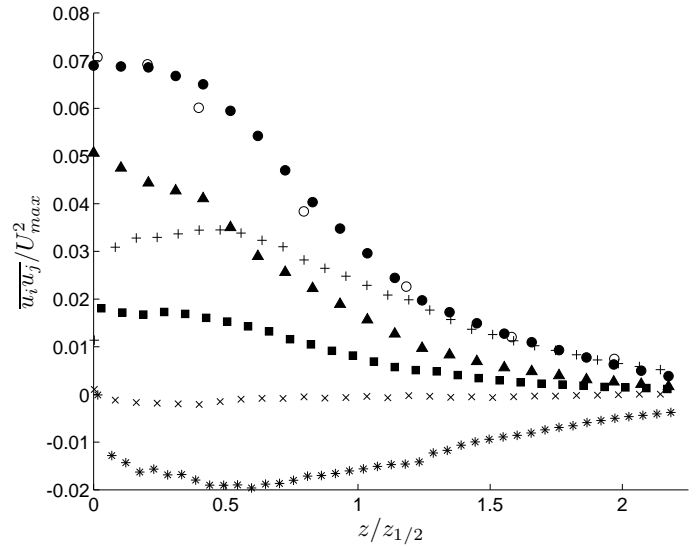


FIGURE 10. Profiles of the normalized Reynolds stresses at y_{max} : (●) \overline{uu} , (○) \overline{uu} PHWA [7], (▲) \overline{uv} , (+) \overline{vw} , (x) \overline{vw} , (■) \overline{vw} , and (*) $\overline{v^2} - \overline{w^2}$.

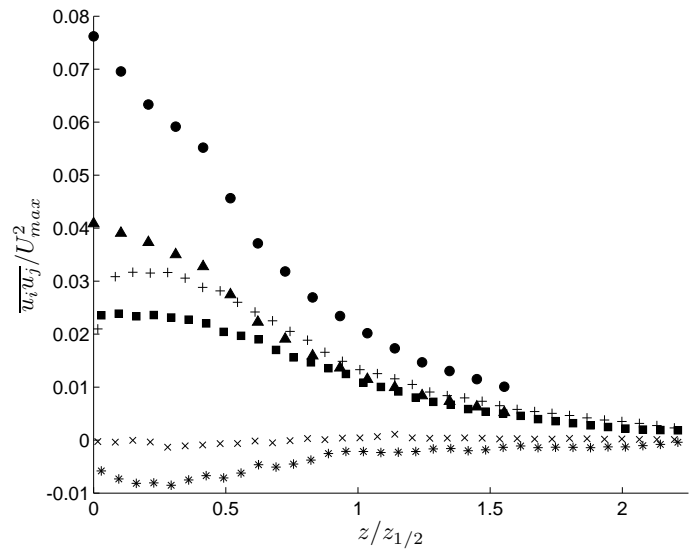


FIGURE 11. Profiles of the normalized Reynolds stresses at $y_{1/2}$: (●) \overline{uu} , (▲) \overline{uv} , (+) \overline{vw} , (x) \overline{vw} , (■) \overline{vw} , and (*) $\overline{v^2} - \overline{w^2}$.

- [7] Venas, B., Abrahamsson, H., Krogstad, P., and Lofdahl, L., 1999. "Pulsed hot-wire measurements in two- and three-dimensional wall jets". *Experiments in Fluids*, **27**, pp. 210–218.
- [8] Hall, J. W., and Ewing, D., 2007. "The development of three-dimensional turbulent wall jets issuing from moderate aspect ratio rectangular channels". *AIAA Journal*, **45**(6), pp. 1177–1186.

- [9] Matsuda, H., Iida, S., and Hayakawa, M., 1990. “Coherent structures in three-dimensional wall jet”. *Transactions of the ASME: Journal of Fluids Engineering*, **112**, pp. 462–467.
- [10] Ewing, D., and Pollard, A., 1997. “Evolution of the large-scale motions in a three-dimensional wall jet”. In 28th AIAA Fluid Dynamics Conference/4th AIAA Shear Flow Control Conference. Paper No. 97-1964.
- [11] Sun, H., and Ewing, D., 2002. “Development of the large-scale structures in the intermediate region of the three-dimensional wall jet”. In Proceedings of the Fluids Engineering Division Summer Meeting, Montreal, ASME. Paper Number FEDSM2002-31414.
- [12] Hall, J. W., and Ewing, D., 2006. “A combined spatial and temporal decomposition of the coherent structures in the three-dimensional wall jet”. In 44th AIAA Aerospace Sciences Meeting and Exhibit, 9–12 Jan 2006, Reno, Nevada, AIAA. Paper Number: AIAA2006-308.
- [13] Hall, J. W., and Ewing, D., 2007. “The asymmetry of the large-scale structures in turbulent three-dimensional wall jets exiting long rectangular channels”. *Journal of Fluids Engineering*, **129**, pp. 929–941.
- [14] Hall, J. W., and Ewing, D., 2010. “Spectral linear stochastic estimation of the turbulent velocity in a square three-dimensional wall jet”. *Journal of Fluids Engineering*, **132**(5), p. 051203.
- [15] LaVision, 2007. *Product Manual– Flow Master*. LaVision GmbH, Germany.
- [16] Lavoie, P., Avallone, G., Gregorio, F. D., Romano, G. P., and Antonia, R. A., 2007. “Spatial resolution of PIV for the measurement of turbulence”. *Experiments in Fluids*, **43**, pp. 39–51.
- [17] Abrahamsson, H., Johansson, B., and Lofdahl, L., 1997. The turbulence field of a fully developed three-dimensional wall jet. Tech. Rep. 91-1, Chalmers University of Technology, Sweden.

ACKNOWLEDGMENT

The authors are grateful for the financial support of the Natural Sciences and Engineering Council of Canada and Druk Green Power Corporation Ltd., Bhutan.